# A Comparison of Structures and Optoelectronic Properties of Oxygen- and Sulfur-Containing Heterocycles: Conjugated Nonylbisoxazole and Nonylbithiazole Oligomers

Jeffrey K. Politis, Fernando B. Somoza, Jr., Jeff W. Kampf, and M. David Curtis*

*Department of Chemistry and the Macromolecular Science and Engineering Center, The University of Michigan, Ann Arbor, Michigan 48109-1055*

L. González Ronda and David C. Martin

*Department of Materials Science and Engineering and the Macromolecular Science and Engineering Center, The University of Michigan, Ann Arbor, Michigan 48109-1055*

*Received May 11, 1999*

The synthesis and characterization of 4,4′-dinonyl-2,2′-bisoxazole (NBO) and its oligomers are described. The optical, electronic, and structural properties of these oligomers, NBO, $NBO_2$, and $NBO_3$, are compared to their sulfur analogues (NBT, $NBT_2$, and $NBT_3$). In the series $(NBO)_n$ and $(NBT)_n$, there is a red shift in the $\lambda_{max}$ as "*n*" increases. This effect is observed in both the solid and solution states. The bithiazole oligomers have longer wavelength absorbances than those of the bisoxazole oligomers; however, the observed red shift is greater as "*n*" increases for the bisoxazole oligomers leading to a merging of the absorption maxima between the two systems. The larger red shift for the bisoxazole series is explained by the larger atomic orbital coefficients at the coupling sites of the bisoxazole oligomers versus those of the bithiazole derivatives. Both systems exhibit thermochromic behavior corresponding to a transition from an ordered to disordered state. Upon heating, the bisoxazole system shows a gradual conformational change indicated by continual blue shifts of the absorption maximum. Conversely, the less rigid bithiazole system exhibits an immediate order−disorder transition upon heating evidenced by the appearance of an isosbestic point in the absorption spectrum. The solid-state packing of the $n = 2$ and 3 oligomers is very similar; however, the solid-state structures of NBO and NBT are different as determined by single-crystal X-ray diffraction. NBO packs in a two-layered "ribbonlike" structure, whereas NBT forms molecular stacks. The reduction potentials of $(NBO)_n$ increase (become more positive) from −2.97 to −2.60 to −2.46 V for $n = 1$, 2, and 3, respectively, and the number of reductions observed corresponds to the number of NBO units.

## Introduction

Conjugated polymers have gained much attention in recent years in large part because of their potential use in several device applications, including light-emitting diodes (LEDs)[1−7] and field effect transistors (FETs).[8−14] Modifications of a polymer must be made to fit each device application. For example, FETs require high mobility of electrons. Recently it was shown that $\pi$-stacking, i.e., overlap of the $\pi$-electron clouds between polymer chains, increases electron mobility by decreasing the energy required for interchain hopping.[15,16] However, the $\pi$-stacked molecules are aligned so as to allow for excimer formation leading to low luminescence efficiencies and poorly performing LEDs.[17] Hence, tun-

* To whom correspondence should be addressed.

(1) Burroughs, J. H.; Bradley, D. D. C.; Brown, A. R.; Marks, R. N.; Friend, R. H.; Burn, P. L.; Holmes, A. B. *Nature* **1990**, *347*, 539.
(2) Brutting, W.; Buchwald, W.; Egerer, G.; Meier, M.; Zuleeg, K.; Schwoerer, M. *Synth. Met.* **1997**, *84*, 677.
(3) Hu, B.; Karasz, F. E.; Morton, D. C.; Sokolik, I.; Yang, Z. *J. Lumin.* **1994**, *60−61*, 919.
(4) Inganäs, O.; Berggren, M.; Andersson, M. R.; Gustafsson, G.; Hjertberg, T.; Wennerstrom, O.; Dyreklev, P.; Granstrom, M. *Synth. Met.* **1995**, *71*, 2121.
(5) Braun, D.; Heeger, A. J. *Appl. Phys. Lett.* **1991**, *58*, 1982.
(6) Burn, P. L.; Holmes, A. B.; Kraft, A.; Bradley, D. D. C.; Brown, A. R.; Friend, R. H. *J. Chem. Soc., Chem. Commun.* **1992**, 32.
(7) He, Y.; Politis, J. K.; Cheng, H.; Curtis, M. D.; Kanicki, J. *IEEE Trans. Electron Devices* **1997**, *44*, 1282.
(8) Horowitz, G. *Adv. Mater.* **1996**, *8*, 177.
(9) Torsi, L.; Dodabalapur, A.; Rothberg, L. J.; Fung, A. W. P.; Katz, H. E. *Science* **1996**, *272*, 1462.
(10) Hajlaoui, R.; Fichou, D.; Horowitz, G.; Nessakh, B.; Constant, M.; Garnier, F. *Adv. Mater.* **1997**, *9*, 57.
(11) Bao, Z.; Feng, Y.; Dodabalapur, A.; Raju, V. R.; Lovinger, A. J. *Chem. Mater.* **1997**, *9*, 1299.
(12) Horowitz, G.; Garnier, F.; Yassar, A.; Hajlaoui, R.; Kouki, F. *Adv. Mater.* **1996**, *8*, 52.
(13) Dodabalapur, A.; Katz, H. E.; Torsi, L.; Haddon, R. C. *Science* **1995**, *269*, 1560.
(14) Garnier, F.; Hajlaoui, R.; Yassar, A.; Srivatava, P. *Science* **1994**, *265*, 1684.
(15) McCullough, R. D.; Williams, S. P. *J. Am. Chem. Soc.* **1993**, *115*, 11608.
(16) McCullough, R. D.; Tristram-Nagle, S.; Williams, S. P.; Lowe, R. D.; Jayaraman, M. *J. Am. Chem. Soc.* **1993**, *115*, 4910.

10.1021/cm990278u CCC: $18.00 
Published on Web 07/14/1999

ing the properties of conjugated polymers is a focus of many research groups. A variety of methods are used to enhance specific properties, but changing one characteristic generally leads to the altering of others. For example, one method of altering the emission color of a polymer is to disrupt the effective conjugation length, but such disruption also changes the solid-state structure and the charge transport properties of the polymer.[3,6,18−24]

Another method of altering the characteristics of a polymer is by specific atomic replacement in the polymer backbone, i.e., switching a nitrogen for a carbon to convert a poly(3-alkylthiophene) (P3AT) to a poly(alkylbithiazole) (PABT) [25−28] or (para-phenylene vinylene) (PPV) to poly(para-pyridine vinylene) (PyPV).[29,30] In these cases, the introduction of the more electronegative N-atom dramatically changes the electrochemical behavior of the polymers while only slightly altering their optical properties. However, the effects caused by these specific atomic changes are not easily predicted. One method of systematically investigating the effects of changes in the ring atoms and/or side chains is to study the effects caused by these changes in short chain oligomers. Trends found for the oligomers might be extrapolated to the polymer.[31−40] For example, one such study of nonylbithiazole oligomers $(NBT)_n$ provided insight into the characteristics of poly(nonylbithiazole) (PNBT).[38]

Sulfur-containing heterocycles have been studied thoroughly, but there has been much less attention given to the comparable oxygen-containing materials. The switch from the more polarizable sulfur to the more electronegative oxygen has little effect on the overall geometry of the molecule, but may change the solid-state structure considerably, as well as the charge transport, optical, and electrochemical behavior. Herein, the synthesis and characterization of nonylbisoxazole (NBO) oligomers is presented, and a comparison is made to the corresponding NBT oligomers.

## Experimental Section

**Materials.** All manipulations and polymerizations were performed under a nitrogen atmosphere using standard Schlenk line techniques unless otherwise stated. Reagents were purchased and used as received unless otherwise stated. The syntheses of 4,4′-dinonyl-2,2′-bithiazole (NBT) and $NBT_3$ were reported[28] previously and the synthesis of $NBT_2$ is contained in the Supporting Information.

$^1$H NMR spectra were collected on a Bruker AM-360, AM-300, or AM-200 and referenced to the residual proton solvent resonance. UV−vis spectra were collected on a Shimadzu 3101PC with baseline correction. Emission spectra were collected on a Shimadzu 4121 interfaced with a Gateway computer. X-ray diffraction (XRD) data were obtained on a Rigaku Rotaflex Diffractometer operated at 40 kV, 100 mA, equipped with a Cu target (0.154 nm) and a graphite monochromator. Samples were scanned from 3 to 35° ($2\theta$) at 0.01° intervals and a rate of 1°/min. The differential scanning calorimetry (DSC) was performed on a Perkin-Elmer DSC 7. Cyclic voltammagrams (CV) were obtained with a home-built potentiostat, designed by W. Burkhardt, Electronics shop, Department of Chemistry, University of Michigan, interfaced to a PC computer with a custom program written by Dr. S. Paras, Department of Chemistry, University of Michigan. The solvent was dry $CH_2Cl_2$, and the supporting electrolyte was tetrabutylammonium hexafluorophosphate (0.1 M). The reported potentials are versus the ferrocene/ferrocenium ($Fc/Fc^+$) couple, obtained by adding a crystal of ferrocene to the analyte solution. Elemental analyses were performed by either Galbraith Laboratories or the University of Michigan Microanalysis Laboratory. Gel permeation chromatography (GPC) was performed using a UV detector and polystyrene calibration standards.

All of the theoretical calculations were conducted on a Macintosh computer with the Cache version 3.8 suite of programs. Extended Hückel calculations were used to calculate molecular orbitals. MOPAC, utilizing the PM3 parameters, was used to optimize the geometry, and Zindo, with INDO/1 parameters and configuration interaction set to 9, was used to calculate the electronic spectrum.

**Synthesis of 1-(Formyloxy)-undecanone.**[41] A 250 mL Schlenk flask equipped with a stir bar and $N_2$ inlet/outlet was charged with 1-bromoundecanone (16.08 g, 64.5 mmol) and sodium formate (5.71 g, 83.9 mmol) in dimethylformamide (DMF) (130 mL), and the mixture was allowed to stir overnight. The light golden brown mixture was poured over ice/$H_2O$ (400 mL). The white solid was collected, washed with $H_2O$ to remove excess DMF, and dried under vacuum. Yield 12.63 g (91.3%). $^1$H NMR ($CDCl_3$): $\delta$ 0.88 (3H, t, $J = 6.4$ Hz, $-CH_3$), 1.22−1.40 (12H, m, $-(CH_2)_6CH_3$), 1.62 (2H, m, $J = 7.2$ Hz, $COCH_2CH_2$), 2.44 (2H, t, $J = 7.4$ Hz, $COCH_2$), 4.75 (2H, s, $-OCH_2$), 8.16 (1H, s, aldehyde). FT-IR (KBr): $\nu_{CO} = 1729$ cm$^{-1}$, 1711 cm$^{-1}$.

**Synthesis of 4-Nonyloxazole.**[41] A 250 mL Schlenk flask equipped with a stir bar, condenser, and $N_2$ inlet/outlet was charged with 1-(formyloxy)-undecanone (11.52 g, 46.2 mmol) in acetic acid (120 mL). The solution was refluxed for 1.75 h,

(17) Conwell, E. *TRIP* **1997**, *5*, 218.
(18) Burn, P. L.; Holmes, A. B.; Kraft, A.; Bradley, D. D. C.; Brown, A. R.; Friend, R. H.; Gymer, R. W. *Nature* **1992**, *356*, 47.
(19) Kraft, A.; Burn, P. L.; Holmes, A. B. *Synth. Met.* **1993**, *55*−*57*, 936.
(20) Holmes, A. B.; Bradley, D. D. C.; Brown, A. R.; Burn, P. L.; Burroughes, J. H.; Friend, R. H.; Greenham, N. C.; Gymer, R. W.; Halliday, D. A.; Jackson, R. W.; Kraft, A.; Martens, J. H. F.; Pichler, K.; Samuel, I. D. W. *Synth. Met.* **1993**, *55*−*57*, 4031.
(21) Hu, B.; Karasz, F. E. *Synth. Met.* **1998**, *92*, 157.
(22) Hay, M.; Klavetter, F. L. *J. Am. Chem. Soc.* **1995**, *117*, 7112.
(23) Kim, H. K.; Ryu, M.; Kim, K.; Lee, S. *Macromolecules* **1998**, *31*, 1114.
(24) Zyung, T.; Hwang, D.; Kang, I.; Shim, H.; Hwang, W.; Kim, J. *Chem. Mater.* **1995**, *7*, 1499.
(25) Yamamoto, T.; Komarudin, D.; Arai, M.; Lee, B. L.; Suganuma, H.; Asakawa, N.; Inoue, Y.; Kubota, K.; Sasaki, S.; Fukuda, T.; Matsuda, H. *J. Am. Chem. Soc.* **1998**, *120*, 2047.
(26) Yamamoto, T.; Suganuma, H.; Maruyama, T.; Inoue, T.; Muramatsu, Y.; Arai, M.; Komarudin, D.; Ooba, N.; Tomaru, S.; Sasaki, S.; Kubota, K. *Chem. Mater.* **1997**, *9*, 1217.
(27) Politis, J. K.; Curtis, M. D.; Gonzalez, L.; Martin, D. C.; He, Y.; Kanicki, J. *Chem. Mater.* **1998**, *10*, 1713.
(28) Nanos, J. I.; Kampf, J. W.; Curtis, M. D.; Gonzalez, L.; Martin, D. C. *Chem. Mater.* **1995**, *7*, 2232.
(29) Li, X.; Cacialli, F.; Cervini, R.; Holmes, A. B.; Moratti, S. C.; Grimsdale, A. C.; Friend, R. H. *Synth. Met.* **1997**, *84*, 159.
(30) Onoda, M.; MacDiarmid, A. G. *Synth. Met.* **1997**, *91*, 307.
(31) Distefano, G.; Jones, D.; Guerra, M.; Favaretto, L.; Modelli, A.; Mengoli, G. *J. Phys. Chem.* **1991**, *95*, 9746.
(32) Faid, K.; Leclerc, M. *J. Chem. Soc., Chem. Commun.* **1993**, 962.
(33) Hernandez, V.; Veronelli, M.; Favaretto, L.; Lopez Navarrete, J. T.; Jones, D.; Zerbi, G. *Acta Polym.* **1996**, *47*, 62.
(34) Hill, M. G.; Penneau, J. F.; Zinger, B.; Mann, K. R.; Miller, L. L. *Chem. Mater.* **1992**, *4*, 1106.
(35) Liao, J.-H.; Benz, M.; LeGoff, E.; Kanatzidis, M. G. *Adv. Mater.* **1994**, *6*, 135.
(36) Pernaut, J. M.; Audebert, P.; Hapiot, P.; Garcia, P. *J. Braz. Chem. Soc.* **1994**, *5*, 127.
(37) Zotti, G.; Schiavon, G.; Berlin, A.; Pagani, G. *Chem. Mater.* **1993**, *5*, 620.
(38) Curtis, M. D.; Cheng, H. T.; Nanos, J. I.; Nazri, G. A. *Macromolecules* **1998**, *31*, 205.
(39) Bidan, G.; De Nicola, A.; Enee, V.; Guillerez, S. *Chem. Mater.* **1998**, *10*, 1052.
(40) Stalmach, U.; Detert, H.; Meier, H.; Gebhardt, V.; Haarer, D.; Bacher, A.; Schmidt, H. W. *Opt. Mater.* **1998**, *9*, 77.
(41) Whitney, S. E.; Winters, M.; Rickborn, B. *J. Org. Chem.* **1990**, *55*, 929.

and the darker solution was poured into $H_2O$ (500 mL). The product was extracted with $CH_2Cl_2$, and washed with $NaHCO_3$ (saturated, 3 × 100 mL) and $H_2O$ (100 mL). The organic layer was dried over $MgSO_4$ and the solvent was removed to give a brown liquid. The liquid was fractionally distilled under vacuum (~0.05 Torr) at 58−60 °C to give a clear liquid. Yield 3.57 g (31.0%). $^1$H NMR ($CDCl_3$): $\delta$ 0.88 (3H, t, $J$ = 6.4 Hz, $-CH_3$), 1.20−1.45 (12H, m, $-(CH_2)_6CH_3$), 1.63 (2H, m, $J$ = 7.3 Hz, ring$-CH_2CH_2$), 2.53 (2H, t, $J$ = 7.1 Hz, ring$-CH_2$), 7.38 (1H, m, $J$ = 1.0 Hz, proton at the 5-position of the ring), 7.80 (1H, s, proton at the 2-position of the ring). GC−MS shows two peaks: undecanone (6%) and 4-nonyloxazole (94%, $M^+$ = 195). UV−vis ($CHCl_3$) = 243 nm.

**Synthesis of 4,4′-Dinonyl-2,2′-bisoxazole (NBO).** A dry 100 mL Schlenk flask equipped with a stir bar and $N_2$ inlet/outlet was charged with 4-nonyloxazole (3.57 g, 18.3 mmol) in dry tetrahydrofuran (THF) (20 mL), and the solution was cooled to −78 °C. The oxazole precipitated and dry tetrahydrofuran (THF) (40 mL) was added. BuLi (2.5 M in hexanes, 7 mL, 17.4 mmol) was added slowly via a syringe. The solution was stirred at −78 °C for 3.5 h. Anhydrous $CuCl_2$ (4.91 g, 36.5 mmol) was added as a solid, and the reaction mixture was stirred at room-temperature overnight. The mixture was poured over crushed ice and extracted with $CHCl_3$. The organic layer was washed with $NH_4OH$ (28%, 2 × 150 mL), $H_2O$ (2 × 200 mL), and dried over $MgSO_4$. The solvent was removed to give a slightly yellow oil which solidified upon standing. The solid was crystallized from $CH_3CN$ to give a lightly colored solid. Yield 1.72 g (48.4%). $^1$H NMR ($CDCl_3$): $\delta$ 0.87 (6H, t, $J$ = 6.5 Hz, $-CH_3$), 1.10−1.40 (24H, m, $-(CH_2)_6CH_3$), 1.68 (4H, m, $J$ = 7.2 Hz, ring$-CH_2CH_2$), 2.59 (4H, t, $J$ = 7.6 Hz, ring$-CH_2$), 7.49 (2H, s, ring protons). $^{13}$C NMR ($CDCl_3$): 14.06, 22.64, 26.24, 28.21, 29.16, 29.25, 29.31, 29.46, 31.84, 135.32, 143.34, 150.90. $\lambda_{max}$ (abs) = 286 nm ($CHCl_3$); 275 nm (film). $\lambda_{max}$ (em) = 329, 343 nm ($CHCl_3$); 331, 343 nm (film). Anal. Calcd. for $C_{24}H_{40}N_2O_2$: C, 74.16; H, 10.39; N, 7.21. Found: C, 74.32; H, 10.26; N, 7.19.

**Synthesis of 5,5′-Diiodo-4;4′-dinonyl-2,2′-bisoxazole ($I_2$-NBO).**[42] A 100 mL Schlenk flask equipped with a stir bar and $N_2$ inlet/outlet was charged with NBO (1.05 g, 2.7 mmol) and silver trifluoroacetate (1.31 g, 5.94 mmol) in $CH_2Cl_2$ (20 mL). $I_2$ (1.51 g, 5.94 mmol) in $CH_2Cl_2$ (40 mL) was added, and the mixture was allowed to stir overnight. The mixture was filtered to remove AgI and the filtrate was washed with $Na_2S_2O_3$ (saturated, 100 mL) and $NaHCO_3$ (saturated, 100 mL), and dried over $MgSO_4$. The solvent was removed to give a yellow oil which solidified upon standing. The solid was recrystallized from $CH_3CN$ to give light yellow crystals. Yield 1.20 g (69.3%). $^1$H NMR ($CDCl_3$): $\delta$ 0.87 (6H, t, $J$ = 6.4 Hz, $-CH_3$), 1.10−1.40 (24H, m, $-(CH_2)_6CH_3$), 1.67 (4H, m, $J$ = 7.1 Hz, ring$-CH_2CH_2$), 2.53 (4H, t, $J$ = 7.5 Hz, ring$-CH_2$). Anal. Calcd. for $C_{24}H_{38}N_2O_2I_2$: C, 45.01; H, 5.99; N, 4.38. Found: C, 45.37; H, 6.14; N, 4.19. MS (EI): $M^+$ = 640.

**Synthesis of 5-Trimethylstannyl-4;4′-dinonyl-2,2′-bisoxazole ($Me_3Sn$−NBO).** A dry 250 mL Schlenk flask equipped with a stir bar and $N_2$ inlet/outlet was charged with dry THF (50 mL), and cooled to −78 °C. BuLi (2.5 M in hexanes, 0.98 mL, 2.44 mmol) was added. NBO (1.00 g, 2.57 mmol) in dry THF (60 mL) was added dropwise via cannula. The yellow mixture was maintained at −78 °C for 5 h and warmed to −25 °C for 1 h, at which time the solution turned dark. The reaction mixture was cooled to −78 °C and trimethyltin chloride (0.61 g, 3.08 mmol) in dry THF (20 mL) was added. The reaction mixture was stirred overnight, and the red-brown solution was washed with $NH_4Cl$ (saturated, 100 mL), $K_2CO_3$ (saturated, 100 mL), and NaCl (saturated, 100 mL). The organic layer was dried over $MgSO_4$ and heated over decolorizing carbon. The solvent was removed in vacuo to give an oily solid. The product was extracted with cold $CH_3CN$. The $CH_3CN$ was removed to give the product as an oily solid. NMR showed the product to be 90% pure (the impurity is NBO). Yield 0.70 g (49.4%). $^1$H NMR ($CDCl_3$): $\delta$ 0.42 (9H, s, $Sn(CH_3)_3$, 0.87 (6H, t, $J$ = 6.5 Hz, $-CH_3$), 1.15−1.48 (24H, m, $-(CH_2)_6CH_3$), 1.68 (4H, overlaid m, ring$-CH_2CH_2$), 2.55 (2H, t, $J$ = 8.0 Hz, ring$-CH_2$ (closest to the Sn)), 2.59 (2H, t, $J$ = 8.0 Hz, ring$-CH_2$ (farthest from Sn)), 7.47 (1H, s, ring proton).

**Synthesis of Bis(4,4′-dinonyl-2,2-bisoxazole-5-yl) ($NBO_2$).** A dry 250 mL Schlenk flask equipped with a stir bar, the $N_2$ inlet/outlet was charged with NBO (0.60 g, 1.54 mmol) in dry THF (150), and the solution was cooled to −15 °C. BuLi (2.5 M in hexanes, 0.60 mL, 1.5 mmol) was added, and the dark solution was stirred at 0 °C for 3 h and cooled to −78 °C for 45 min. $CuCl_2$ (0.41 g, 3.08 mmol) was added as a solid, and the mixture was allowed to stir at room-temperature overnight. The mixture was poured over ice and extracted with $CHCl_3$. The organic layer was washed with $NH_4OH$ (28%, 2 × 150 mL), $H_2O$ (2 × 200 mL), and dried over $MgSO_4$. Removal of solvent gave a yellow solid. The dimer was extracted with MeOH from the mixture in a Soxhlet apparatus. Cooling the MeOH solution gave a yellow precipitate which was filtered and dried. Yield 0.28 g (46.7%). $^1$H NMR ($CDCl_3$): $\delta$ 0.80−0.95 (12H, overlapping triplets, $-CH_3$), 1.20−1.50 (48H, m, $-(CH_2)_6CH_3$), 1.55−1.93 (8H, m, ring$-CH_2CH_2$), 2.62 (4H, t, outer rings$-CH_2$, $J$ = 7.6 Hz), 2.83 (4H, t, inner rings$-CH_2$, $J$ = 7.7 Hz), 7.53 (2H, s, ring protons). $\lambda_{max}$ (abs) = 348 nm ($CHCl_3$); 368 nm (film). $\lambda_{max}$ (em) = 396, 420, 441 nm ($CHCl_3$); 484 nm (film). MS(EI): $M^+$ = 774.8.

**Synthesis of 5,5′-Bis(4,4′-dinonyl-2,2′-bisoxazole-5-yl)-4,4′-Dinonyl-2,2′-bisoxazole ($NBO_3$).** A dry 50 mL Schlenk flask equipped with a stir bar and $N_2$ inlet/outlet was charged with $Me_3Sn$−NBO (0.70 g, 1.27 mmol), $I_2$−NBO (0.37 g, 0.58 mmol), and $Pd(PPh_3)_2Cl_2$ (0.02 g, 0.023 mmol) in dry THF (20 mL). A condenser was added and the reaction mixture was heated to reflux. After 23 h, $Pd(PPh_3)_2Cl_2$ (0.01 g, 0.012 mmol) and CuI (0.01 g, 0.05 mmol) were added to the yellow-orange solution and the reaction mixture was heated for another 20 h during which time an orange precipitate formed. The solvent was removed under vacuum to give an orange solid. The solid was stirred in hot MeOH (2 × 150 mL) and filtered. The orange solid was collected and dried under vacuum. Yield 0.34 g (50%). $^1$H NMR ($CDCl_3$): $\delta$ 0.77−1.00 (18 H, overlaid t), 1.10−1.48 (72 H, m), 1.62−1.88 (12 H, m), 2.62 (4 H, t, outer rings$-CH_2$, $J$ = 7.4 Hz), 2.88 (8 H, t, inner rings$-CH_2$, $J$ = 7.5 Hz), 7.53 (2 H, s, ring protons). $\lambda_{max}$ (abs) = 381 nm ($CHCl_3$); 409 nm (film). $\lambda_{max}$ (em) = 466 nm ($CHCl_3$); 533 nm (film). MS(FAB): $M^+$ = 1162.0.

**NBO Structure Determination.** A small, colorless needle of NBO with dimensions 0.20 × 0.20 × <0.01 mm, grown from a solution of THF/$CH_3CN$, was mounted on a Siemens SMART charge-coupled detector (CCD)-based X-ray diffractometer equipped with a normal focus Mo-target X-ray tube ($\lambda$ = 0.71073 A) operated at 2000 W power (50 kV, 40 mA). The X-ray intensities were measured at 158 K with the detector placed at a distance of 5.103 cm from the crystal. A total of 2132 frames were collected with a scan width of 0.3° in $\omega$ and an exposure time of 120 s/frame. The frames were integrated with the Siemens SAINT software package with a narrow frame algorithm. The integration of the data using a triclinic unit cell yielded a total of 9306 reflections to a maximum $2\theta$ value of 46.7° of which 3398 were independent and 1684 were greater than $2\sigma$(I). The final cell constants were based on the *xyz* centroids of 2746 reflections above $10\sigma$(I). Analysis of the data showed negligible decay during data collection. The structure was solved by direct methods and refined with the Siemens SHELXTL (version 5.03) software package. The space group was $P1^-$ with $a$ = 5.7663(5) Å, $b$ = 10.7060(5) Å, $c$ = 19.317(2) Å, $\alpha$ = 90.176(4)°, $\beta$ = 92.566(3)°, $\gamma$ = 97.940(4)°, and $Z$ = 2 for the formula unit $C_{24}H_{40}N_2O_2$. All non-hydrogen atoms were refined anisotropically, and the hydrogen atoms were placed in idealized positions. The final, full matrix refinement on the basis of $F^2$ converged at $R1$ = 0.1069 and w$R2$ = 0.2354 (on the basis of observed data); $R1$ = 0.1965 and w$R2$ = 0.2902 (on the basis of all data). The relatively high residuals are due primarily to the extremely thin dimension of the crystal. The largest peak/hole in the final difference map was +0.33/−0.38 e/Å$^3$.

(42) Sy, W. W.; Lodge, B. A. *Tetrahedron Lett.* **1989**, 3769.

**Scheme 1. Synthesis of 4,4′-Dinonyl-2,2′ Bisoxazole (NBO)**

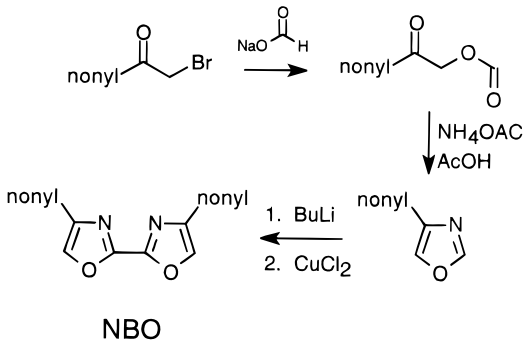


NBO

**Scheme 2. Synthesis of NBO Dimer and Trimer**

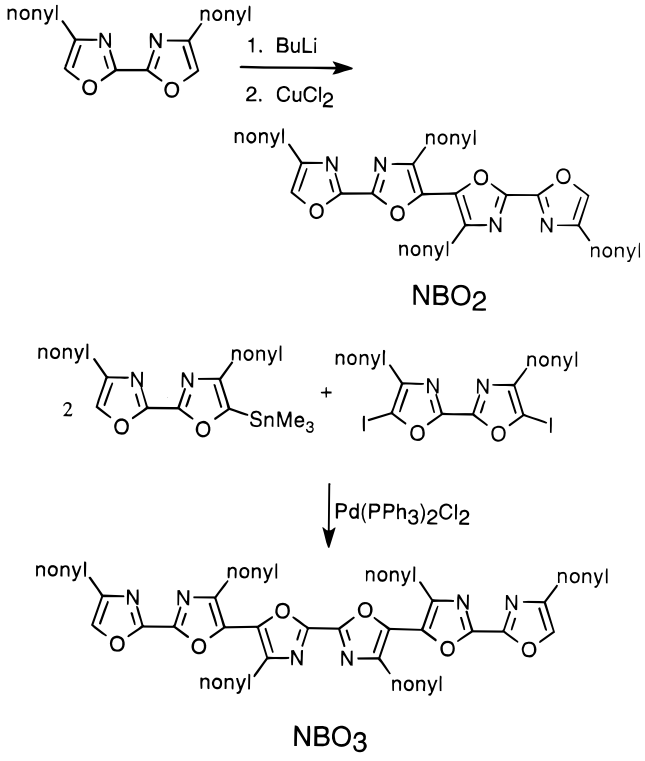


NBO2

NBO3

## Results and Discussion

**Preparation.** The synthesis of NBO is shown in Scheme 1. The first step was the reaction of 1-bromoundecanone with sodium formate to make 1-(formyloxy)-undecanone. Ring closure and dehydration with ammonium acetate in acetic acid affords the 4-nonyloxazole. Deprotonation at −78 °C and subsequent coupling with $CuCl_2$ gives solely NBO, i.e., none of the isomeric 4,4′-dinonyl-5,5′-bisoxazole was observed. Scheme 2 shows the synthesis of the higher-order oligomers. The dimer ($NBO_2$) was synthesized from NBO via a similar coupling routine: monolithiation followed by coupling with $CuCl_2$. A Stille coupling of $Me_3Sn$−NBO with $I_2$−NBO gave the trimer ($NBO_3$).

The chemistry that can be performed with NBO is similar to that of the sulfur derivative, NBT, but the synthetic route used to prepare each compound is different. Although both syntheses begin with 1-bromoundecanone, the synthesis of NBT involves a more direct route: reaction of 1-bromoundecanone with dithiooxamide affords NBT in one step. In contrast, reacting oxamide and 1-bromoundecanone was unsuccessful as a result of the poor nucleophilicity of oxamide. Therefore, the single ring compound, 4-nonyloxazole, was synthesized as a precursor. The nonyl substituent was used for the best direct comparison to the known thiazole systems. However, as with the thiazoles, the ring substituent can be altered by changing the starting 1-bromo-ketone.

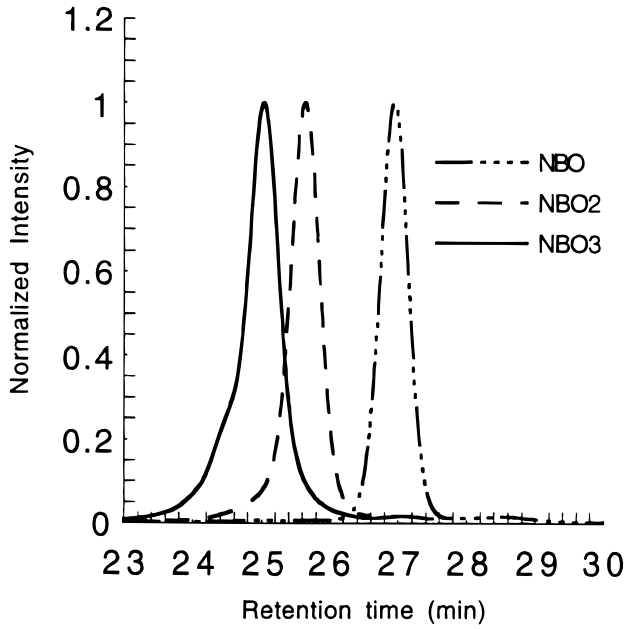


**Figure 1.** GPC traces for NBO, $NBO_2$, and $NBO_3$.

GPC was used to determine the purity of the oligomers. Figure 1 shows the GPC traces of the bisoxazole oligomers. Both NBO and $NBO_2$ are monodisperse, whereas $NBO_3$ has a higher molecular weight shoulder because of the presence of a small amount of tetramer. The molecular weights determined by GPC vs polystyrene standards were 630, 1150, and 1500 for NBO, $NBO_2$, and $NBO_3$, respectively, compared to the actual values of 388, 775, and 1162. The erroneous GPC values of the molecular weight are a function of the conformational differences between the oligomers and the calibration standard, polystyrene. The more extended, rodlike shape of the oligomers as compared to the random coil conformation of polystyrene causes faster retention times and leads to higher calculated molecular weights for the oligomers. Exact molecular weights were obtained by mass spectrometry (see Experimental Section).

The proton NMR spectra provide confirmation of the structures of the oligomers. Figure 2 shows a portion of the NMR spectrum for each oligomer. The α-methylene protons of the nonyl group in NBO appear as one triplet at 2.59 ppm, whereas $NBO_2$ and $NBO_3$ have two types of α-methylene signals, an inner set at 2.83 ppm for $NBO_2$ or 2.88 for $NBO_3$ and an outer set at 2.62 ppm. The two triplets from the α-methylene protons of $NBO_2$ have equal area, whereas $NBO_3$ has an integration of 2:1 from the eight inner and four outer α-methylene protons. The *β*-methylene protons behave similarly, but are not as well resolved.

**Spectral Data.** Figure 3 overlays the solution UV−vis spectra of the oligomers. NBO absorbs at the shortest wavelength, 286 nm. The absorbance red shifts

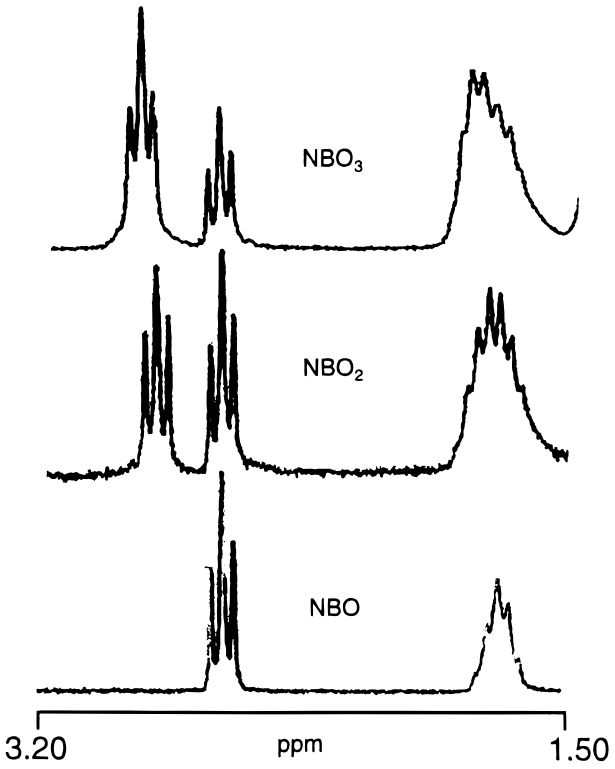


**Figure 2.** Proton NMR spectra of the α- and β-methylene protons for NBO, $NBO_2$, and $NBO_3$.

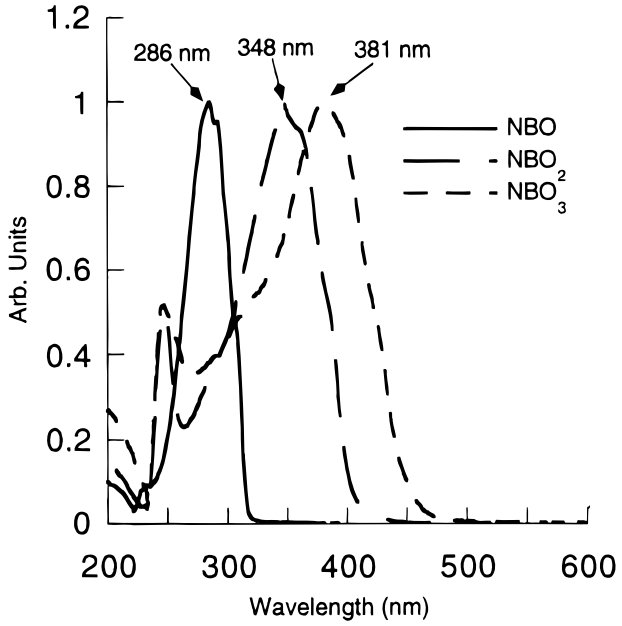


**Figure 3.** The UV−vis spectra of NBO, $NBO_2$, and $NBO_3$ solutions in $CHCl_3$.

upon formation of $NBO_2$, $\lambda_{max} = 348$ nm, and again with $NBO_3$, $\lambda_{max} = 381$ nm. Thus, the effective conjugation length increases with increasing number of NBO units. Figure 4 is a plot of the UV−vis spectra of the oligomer films. The solid-state absorbance exhibits the same trend; however, the maxima are shifted with respect to their values in solution. NBO blue shifts to an absorbance maximum at 275 nm. Both $NBO_2$ and $NBO_3$ red shift in the films to 368 and 409 nm, respectively.

The solid-state UV−vis absorptions of conjugated oligomers are typically red-shifted from the $\lambda_{max}$ of the

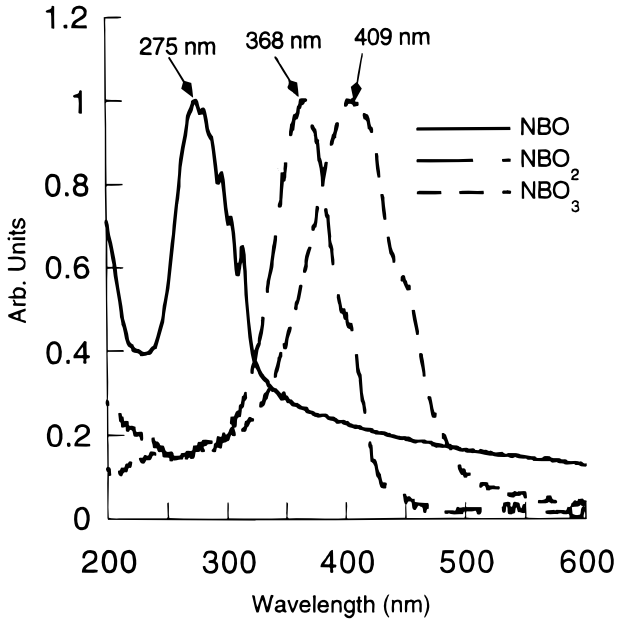


**Figure 4.** The UV−vis spectra of NBO, $NBO_2$, and $NBO_3$ solid films.

solution. For example, in regioregular poly(3-alkylthiophene) where the solid state conformation is known to be planar,[15,16,43] red shifts in the $\lambda_{max}$ of the UV−vis spectra of up to ca. 100 nm were observed in going from solution to the film.[43] However, the extent (and even the direction) of the shift in $\lambda_{max}$ depends on two factors: the first is related to changes in molecular conformations in the solution vs the solid state; the second effect arises from perturbations on the "molecular" $\pi-\pi^*$ transition by neighboring molecules. The effects caused by differences in molecular conformations is generally well known. In a good solvent, the molecular conformations are disordered and the rings in the polymer/oligomer backbone are twisted from coplanarity because of the relatively modest rotational barriers about the single bonds that join the rings, and the flexibility inherent in the alkyl side chains. The solid-state conformations are driven by the dynamics of the molecular packing which favor a planarization of the backbone and promote the fully extended zigzag conformation of the alkyl side chains. The planar backbone with extended side chains allows the most dense molecular packing. The planarization also increases the p-orbital overlap between rings, thereby increasing the effective conjugation length and the absorption wavelength. As the solid-state conformation and solution conformation become more similar, the difference in the $\lambda_{max}$ between the solution and solid decreases. For instance, an increase in the number of random head-to-head couplings in P3AT decreases the solid-state order until the polymer becomes amorphous. The UV−vis maximum of this disordered solid is only 10 nm red-shifted from the polymer solution.[43]

The second solid-state effect on the absorption spectrum is caused by intermolecular interactions. Stacking the planar backbones gives rise to "aggregates", of which there are two types.[44] Face-to-face stacking is referred

(43) Chen, T.-A.; Wu, X.; Rieke, R. D. *J. Am. Chem. Soc.* **1995**, *117*, 233.

**Table 1. Summary of the Optical Data**

| oligomer | $\lambda_{max}$ (abs, nm) solution ($CHCl_3$) | $\lambda_{max}$ (abs, nm) film |
|---|---|---|
| NBO | 286 | 275 |
| $NBO_2$ | 348 | 368 |
| $NBO_3$ | 381 | 409 |
| NBT | 333 | 333 |
| $NBT_2$ | 365 | 409 |
| $NBT_3$ | 381 | 446 |

to as an "H-aggregate", and these give rise to a blue shift in $\lambda_{max}$ as compared to the isolated molecule. End-to-end or "staircase" stacking leads to "J-aggregates" that cause a red shift in $\lambda_{max}$. Thus, the shift in $\lambda_{max}$ between the solution and solid state of conjugated oligomers is the combined result of two effects: planarization of the molecule with its associated increase in conjugation length, and intermolecular aggregation phenomena. Planarization always leads to a red shift, but the direction of shift caused by aggregation depends on the details of the molecular packing in the solid state. For most systems of conjugated rings, the effect of planarization dominates and $\lambda_{max}$ (solid) > $\lambda_{max}$ (solution). However, if the solution and solid-state conformations are very similar (as is believed to be true with NBO), then the effect of aggregation dominates the shift in $\lambda_{max}$ and a blue shift is observed as a consequence of the face-to-face stacking seen in the solid-state structure of NBO (see below). Blue shifts were calculated for confacial stilbene dimers,[45] and blue shifts were observed for alkoxy-substituted PPV oligomers.[40] Even when the effect of planarization dominates the overall red shift in $\lambda_{max}$, aggregation causes "fine structure" or shoulders to appear on the main $\pi-\pi^*$ absorption peak.[46]

Table 1 summarizes the optical data for $NBO_n$ and $NBT_n$. The $\lambda_{max}$ red shifts by 20 and 28 nm from solution to the film for $NBO_2$ and $NBO_3$, respectively. The corresponding shifts for the thiazole system are 44 nm, from 365 (solution) to 409 nm (film) for $NBT_2$, and 65 nm, from 381 (solution) to 446 nm (film), for $NBT_3$.[38] All of the solid-state spectra exhibit the shoulders characteristic of aggregation effects. The solid-state conformations of both sets of oligomers are believed to have planar backbones by virtue of the longer wavelength absorbances seen in the films as well as the X-ray crystal structures (see below). The smaller changes in the absorption maxima of the oxazole oligomers indicate a closer resemblance of their solution conformations compared to those in the solid state. Hence, $NBO_n$ oligomers appear to have more planar molecular conformations in solution than their bithiazole counterparts.

Molecular orbital (MO) calculations were used to explore the dependence of $\lambda_{max}$ on the chain length. We found that a simple model can be used to explain the apparent saturation of conjugation length with increasing chain length, as well as the relative sensitivities of $\lambda_{max}$ of $NBO_n$ vs $NBT_n$ oligomers to increases in chain length. When two aromatic or heteroaromatic rings are joined together, the MOs on one ring interact with those of the other. Maximum energy dispersion arises when the two interacting MOs are close in energy and when the overlap of the two MOs is large. The latter criterion is satisfied if the interacting MOs have a large atomic orbital (AO) coefficient at the connection points, i.e., the 5,5′-positions of NBO or NBT dimers. Thus, to a first approximation, the highest occupied molecular orbitals (HOMOs) of the separate NBO or NBT units that are joined to form the dimers, $NBO_2$ or $NBT_2$, will interact to form a bonding and an antibonding combination. The antibonding combination will increase in energy and become the HOMO of the dimer. Similarly, the lowest unoccupied molecular orbitals (LUMOs) of the separate NBO or NBT fragments will form bonding and antibonding combinations, and the low energy bonding combination will become the LUMO of $NBO_2$ or $NBT_2$. These relationships are diagrammed in Figure 5. If the energy dispersion is large, as seen in Figure 5(a), then there is a large decrease in the energy of the $\pi-\pi^*$ transition, i.e., there is a large decrease in the optical band gap. Conversely, if the interacting MOs have small AO coefficients at the coupling sites, there is little change in the optical band gap as the chain length increases (Figure 5(b)).

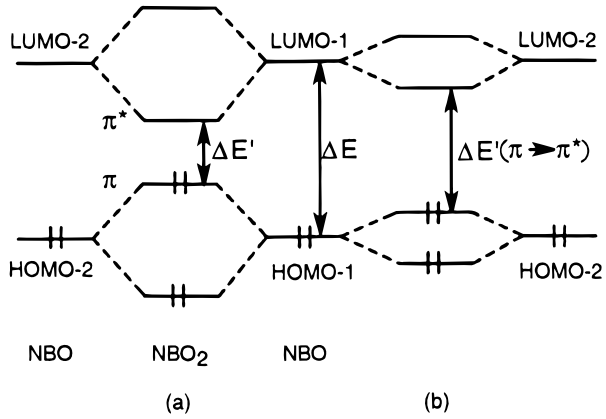


**Figure 5.** (a) Interaction of two HOMOs and two LUMOs of separate rings when there is a large AO coefficient at the coupling position gives a large energy dispersion. (b) Small energy dispersion occurs when there is a small AO coefficient at the coupling position in the interacting MOs.

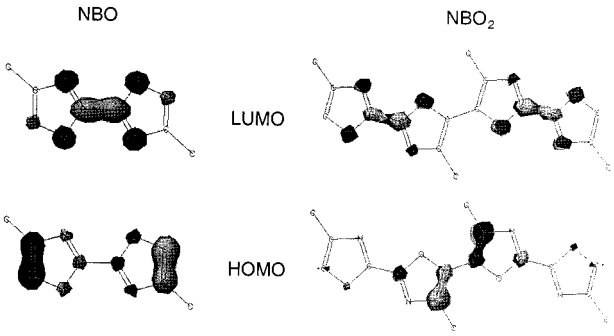


**Figure 6.** Extended Hückel calculated MOs for MBO and $MBO_2$.

Figure 6 shows the Extended Hückel calculated HOMOs and LUMOs for NBO and $NBO_2$. The HOMO and LUMO of NBO have larger AO coefficients at the 5,5′-positions, i.e., the coupling sites, whereas the HOMO and LUMO of $NBO_2$ have nodes at these

(44) (a) Davydov, A. S. *J. Exp. Theor. Phys. (U. S. S. R.)* **1948**, *18*, 210. (b) McRae, E. G.; Kasha, M. *J. Chem. Phys.* **1958**, *28*, 721. (c) *J-Aggregates*; Kobayashi, T., Ed.; World Scientific Publishing Co.: Singapore, 1996. (d) Evans, C. E.; Song, Q.; Bohn, P. W. *J. Phys. Chem.* **1993**, *97*, 12302.

(45) Cornil, J.; dos Santos, D. A.; Crispin, X.; Silbey, R.; Bredas, J. L. *J. Am. Chem. Soc.* **1998**, *120*, 1269.

(46) Koren, A. B.; Curtis, M. D.; Kampf, J. W., submitted for publication.

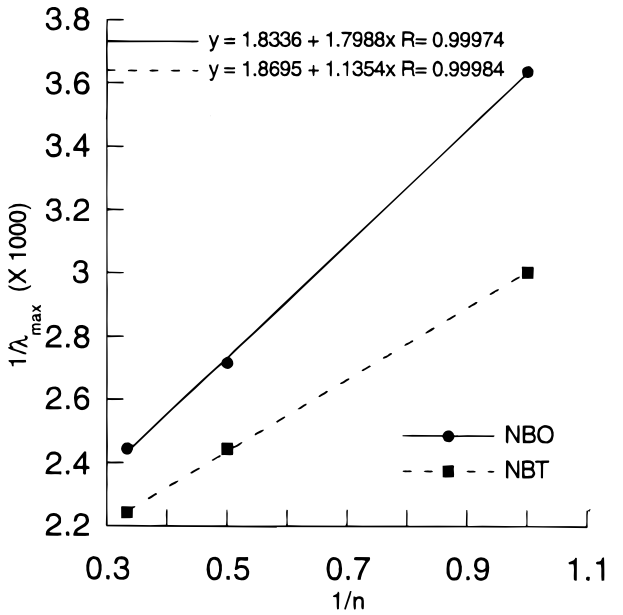


**Figure 7.** Plots of $1/\lambda_{max}$ vs $1/n$ for NBO and NBT oligomers.

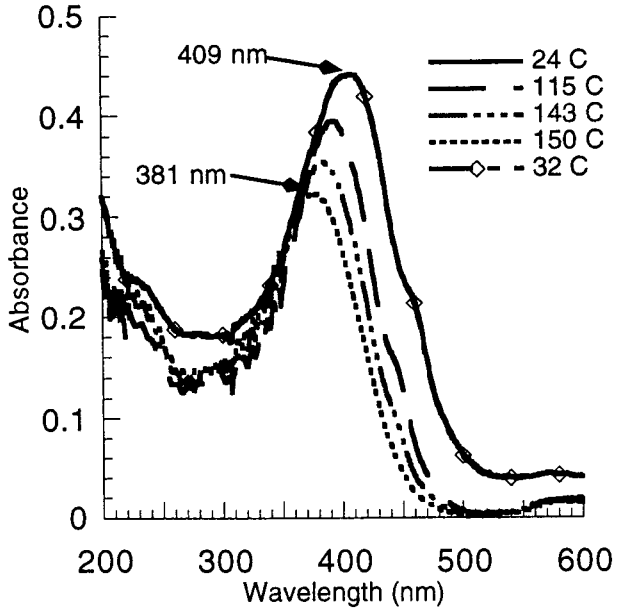


**Figure 8.** UV−vis spectra of an $NBO_3$ film at different temperatures.

positions. Hence, coupling two NBO molecules to give $NBO_2$ will give a large decrease in the $\pi-\pi^*$ transition energy, whereas coupling two $NBO_2$ units to form the tetramer, $NBO_4$, should cause only a very small shift in the $\pi-\pi^*$ transition. Coupling NBO and $NBO_2$ to give the trimer, $NBO_3$, would cause a very modest decrease in $\Delta E(\pi-\pi^*)$. These expectations are borne out experimentally. $\Delta\lambda_{max}$ ($NBO_2-NBO$) is 93 nm (1.14 eV), whereas the shift from $NBO_2$ to $NBO_3$ is only 41 nm (0.34 eV).

The MOs for the bithiazole oligomers are similar to the bisoxazole system and thus, exhibit the same trend. The shift in the solid-state absorption from NBT to $NBT_2$ was 76 nm (0.69 eV), from 333 to 409 nm, and 37 nm (0.25 eV), from 409 to 446 nm, in going from $NBT_2$ to $NBT_3$.[38] Figure 7 is a plot of $1/\lambda_{max}$ vs $1/n$ for both the bisoxazole and bithiazole oligomers. A straight line can be fit for both sets of oligomers. The slopes of the lines indicate that the absorption maximum of the bisoxazole oligomers approaches that of the bithiazole oligomers as the chain length increases. The greater sensitivity of $\lambda_{max}$ on chain length of $(NBO)_n$ vs $(NBT)_n$ is caused by the larger AO coefficients on the 5,5′-positions in the HOMO and LUMO of NBO compared to NBT. Because of the increased delocalization, the AO coefficients at the terminal positions in any oligomeric chain will decrease as the chain length increases (the squares of all the AO coefficients must sum to 1.0 for a normalized MO, hence, as the number of coefficients increases, the average size of any given coefficient will decrease). As the size of the AO coefficients at the coupling positions decreases, the band dispersion also decreases as shown above; and the rate of decrease in optical band gap with increasing chain length becomes very small after the chain length reaches about 4−6 rings.

**Thermochromism.** Figure 8 overlays the UV−vis spectra of an $NBO_3$ film taken at different temperatures. As the temperature increases, the absorbance maximum blue shifts, from 409 to 381 nm, and the intensity decreases. The same behavior is observed for $NBO_2$, which shifts from 368 to 348 nm. In both cases, the shifts occur below the melting points and the final maxima are identical to those of the solution, implying that the conformations at elevated temperatures are identical to those in solution. The gradual shift of the $\lambda_{max}$ is evidence for a transition through multiple conformations. The higher temperatures promote twisting of the rings out of coplanarity causing defects along the conjugated backbone. The loss of planarity shortens the effective conjugation length, and thus a blue shift is observed. The loss in intensity is due to a decrease in the molar absorptivity coefficient caused by a decrease in the transition dipole, which is also a function of conjugation length.

**Table 2. Calculated Transition Moments, Oscillator Strengths, and Wavelengths for $MBO_2$**

| ring twist angle[a] | 0° | 15° | 30° | 45° |
|---|---|---|---|---|
| transition moment[b] | | | | |
| *x* | 2.79 | 2.81 | −2.76 | −2.68 |
| *y* | 9.53 | 9.42 | −9.12 | −8.67 |
| *z* | −0.20 | −0.52 | 1.07 | 1.61 |
| oscillator strength | 1.03 | 1.02 | 0.99 | 0.96 |
| $\lambda_{max}$ (nm) predicted | 454 | 448 | 436 | 418 |

[a] The angle between two planar MBO rings in $MBO_2$. [b] The molecule lies in the *xy*-plane with the long axis in the *y*-direction.

This behavior was modeled with Zindo calculations of methylbisoxazole dimer ($MBO_2$) by changing the angle between MBO units from 180 to 165, 150, and 135°. The modeling shows that twisting the backbone causes a continual shift to higher energy as well as a decrease in intensity. Table 2 lists the predicted absorbances, transition dipoles, and oscillator strengths for the twisted MBO dimers and Figure 9 overlays their calculated electronic spectra.

The NBT oligomer films also blue shift and loose intensity upon heating.[38] The thermochromic behavior of $NBT_3$ is shown in Figure 10. The wavelength shift was not gradual, but rather exhibited an isosbestic point. The existence of an isosbestic point indicates that only two absorbing species coexist; the

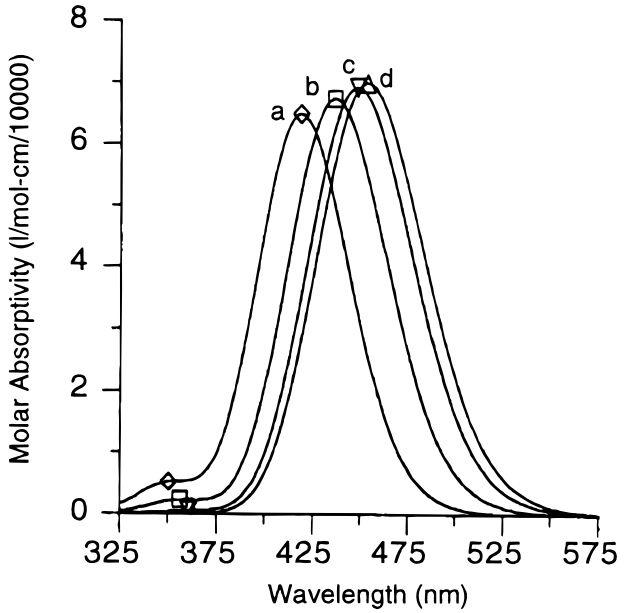


**Figure 9.** Calculated UV−vis spectra for $MBO_2$ for OCCO dihedral angles of (a) 135°, (b) 150°, (c) 165°, and (d) 180° between the two MBO units.

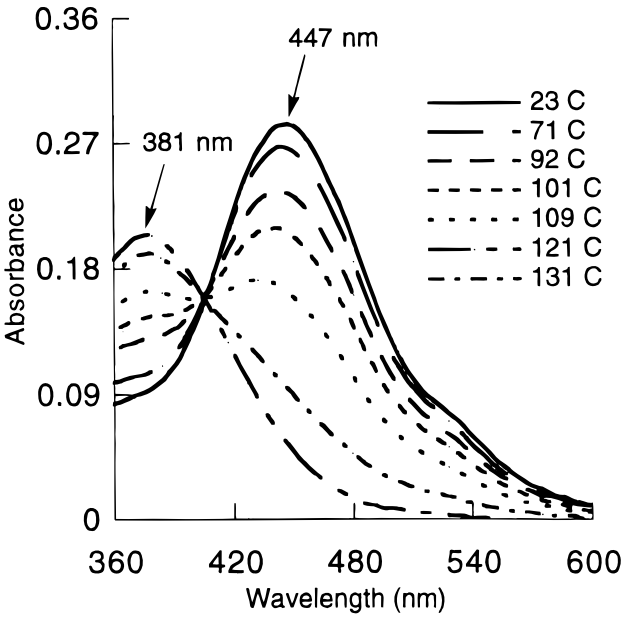


**Figure 10.** UV−vis spectra of an $NBT_3$ film at different temperatures.

planar structure and the disordered, twisted, solution-like structure.

It has been shown in P3ATs that less rigid or less ordered materials exhibit an isosbestic point, whereas a gradual shift was observed for the more rigid, regio-regular polymers with short side chains.[47,48] The NBO oligomers are more rigid than the NBT oligomers as shown by the more planar solution conformation of the former. Hence, the NBO oligomers exhibit gradually increasing ring twists and defect formation with the increasing temperature, whereas the NBT oligomers show a cooperative, order−disorder transition.

(47) Faid, K.; Frechette, M.; Ranger, M.; Mazerolle, L.; Levesque, I.; Leclerc, M.; Chen, T.-A.; Rieke, R. D. *Chem. Mater.* **1995**, *7*, 1390.
(48) Yang, C.; Orfino, F. P.; Holdcroft, S. *J. Am. Chem. Soc.* **1996**, *29*, 6510.

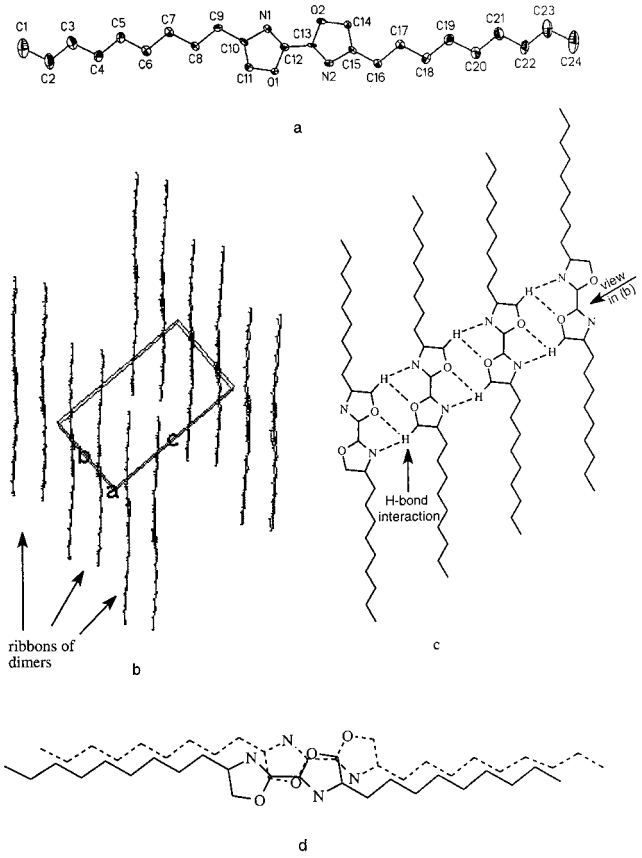


**Figure 11.** (a) ORTEP view of the molecular structure with the atomic numbering scheme. (b) View down the axis of the two-layered ribbons, shown at right angles in (c). Molecules in one layer of the ribbon lie over a second layer to form "$\pi$-dimers" shown in (d).

**Thermal Analysis.** The melting points and heats of fusion for $(NBO)_n$ were determined by DSC analysis. The melting points are 81, 128, and 172 °C for NBO, $NBO_2$, and $NBO_3$, respectively. The heat of fusion for NBO is 60.2 kJ/mol, and for $NBO_2$ and $NBO_3$ the values are 38.8 and 58.2 kJ/mol, respectively. The thiazole oligomers have lower melting points and lower heats of fusion than the corresponding oxazole oligomers: $NBT_n$ melt at 59, 77, and 122 °C for $n = 1$, 2, and 3, respectively. The heat of fusion for NBT is 48.2 kJ/mol, 12 kJ/mol less than that determined for NBO. $NBT_2$ and $NBT_3$ have heats of fusion of 14.4 and 22.7 kJ/mol, respectively, which are 24.4 and 35.5 kJ/mol less than that observed for their corresponding bisoxazole derivatives. The higher heats of fusion of the NBO oligomers may also be related to their gradual thermochromic transitions vs the abrupt order−disorder transition of the NBT oligomers. The decrease and subsequent increase of the heats of fusion in going from NBO to $NBO_2$ to $NBO_3$ and in going from NBT to $NBT_2$ to $NBT_3$ may be caused by a change in the relative contributions of the side chains vs the main chain as the molecular shape changes from oblate in the monomer to prolate in the trimer.

**Solid-State Structure.** The solid-state structure of NBO was obtained by single-crystal XRD ($R = 0.1069$). The molecular geometry and the packing of NBO is shown in Figure 11. The molecule adopts a nearly planar, trans-conformation with the alkyl substituents roughly coplanar with the rings. There is an ap-

**Table 3. Selected Bond Lengths, Bond Angles, and Dihedral Angles of NBO**

| bond lengths (Å) | | bond angles (deg) | | dihedral angles (deg) | |
|---|---|---|---|---|---|
| O(1)−C(12) | 1.351(6) | C(12)−O(1)-C(11) | 104.3(4) | O(1)−C(12)-C(13)−O(2) | 173.4 |
| O(1)−C(11) | 1.358(6) | C(12)−N(1)-C(10) | 104.5(4) | N(1)−C(12)-C(13)−N(2) | 173.2 |
| N(1)−C(12) | 1.295(6) | C(1)−C(2)-C(3) | 114.5(5) | N(1)−C(10)-C(11)−O(1) | −0.3 |
| N(1)−C(10) | 1.403(5) | C(2)−C(3)-C(4) | 114.4(5) | C(10)−C(11)-O(1)−C(12) | 0.6 |
| C(1)−C(2) | 1.499(8) | C(5)−C(4)-C(3) | 114.5(4) | C(11)−O(1)-C(12)−N(1) | −0.8 |
| C(2)−C(3) | 1.518(7) | C(6)−C(5)-C(4) | 113.8(4) | O(1)−C(12)-N(1)−C(10) | −0.5 |
| C(3)−C(4) | 1.528(7) | C(5)−C(6)-C(7) | 114.1(4) | C(12)−N(1)-C(10)−C(11) | −0.1 |
| C(4)−C(5) | 1.503(6) | C(8)−C(7)-C(6) | 112.9(4) | C(11)−C(10)-C(9)−C(8) | −5.1 |
| C(5)−C(6) | 1.502(7) | C(9)−C(8)-C(7) | 112.9(4) | N(1)−C(10)-C(9)−C(8) | 177.4 |
| C(6)−C(7) | 1.525(6) | C(10)−C(9)-C(8) | 112.8(4) | C(10)−C(9)-C(8)−C(7) | −179.5 |
| C(7)−C(8) | 1.521(7) | C(11)−C(10)-N(1) | 107.9(4) | | |
| C(8)−C(9) | 1.517(6) | C(11)−C(10)-C(9) | 129.4(4) | | |
| C(9)−C(10) | 1.500(7) | N(1)−C(10)-C(9) | 122.7(4) | | |
| C(10)−C(11) | 1.342(6) | C(10)−C(11)-O(1) | 109.2(4) | | |
| C(12)−C(13) | 1.433(7) | N(1)−C(12)-O(1) | 114.1(4) | | |
| | | N(1)−C(12)-C(13) | 129.6(4) | | |
| | | O(1)−C(12)-C(13) | 116.3(4) | | |

proximate $C_2$-axis perpendicular to the molecular plane giving the molecule an idealized symmetry of $C_{2h}$. Table 3 lists selected bond lengths, bond angles, and dihedral angles of NBO. The dihedral angle for N1−C12−C13−N2 is 173.4° and for N1−C10−C9−C8 is 177.4°. The corresponding angles for NBT were previously determined to be 180.0 and 68.2°, respectively.[28] Hence, the coplanarity of the rings in NBO was expected, but the approximate coplanarity of the nonyl substituent was surprising because the alkyl chains in NBT and alkyl-substituted oligo-thiophenes do not lie in the ring-planes.[28,49] The calculated linear least-squares plane of the NBO molecule has an atomic mean deviation of 0.099 Å with a maximum deviation at C14 of −0.282 Å. The molecular geometry of NBO closely resembles that of 4,4′-bipentoxy-2,2′-bithiophene (PBTh) which has a comparable dihedral angle of 177.9° from the ring to the alkoxy chain.[50]

Unlike NBT and pentoxybithiophene which have monoclinic unit cells, NBO crystallizes in the triclinic $P1^-$ space group with $Z = 2$. Two molecules lie face to face at a distance of 3.38 Å, related by an inversion center. These dimers then form a two-layered "ribbon", one layer of which is shown in Figure 11c (this view is perpendicular to the one shown in Figure 11(b)). The other layer of the double ribbon is the other half of the "dimer" related by the inversion center as shown in Figure 11d. There appear to be weak H-bonds between the N- and O-atoms with the H-atom located on the 5-position on an adjacent molecule in the strands of the ribbon (Figure 11(c)). The N- - -H distance is 2.60 Å and the O- - -H distance is 2.89 Å. The presence of a H-bond would be highly unusual because the H-atom is not bonded to a heteroatom; however, the electron withdrawing nature of the O- and N-atoms within the ring may polarize the C−H bond enough to allow for weak H-bonding interactions. This same effect is believed to exist in other highly polar compounds such as acetonitrile.[51] Nevertheless, the intermolecular distance between dimer stacks seems to be determined by the N- - -H interaction and the O1- - -O2′ contact which has a distance of 2.62 Å, compared to the sum of the van der Waals radii, 2.75 and 3.04 Å, respectively. In contrast, NBT forms infinite, slipped or "staircase $\pi$-stacks" that have short (3.49 Å) interstack S···S contacts (the S···S distance between molecules within a stack is 4.73 Å).

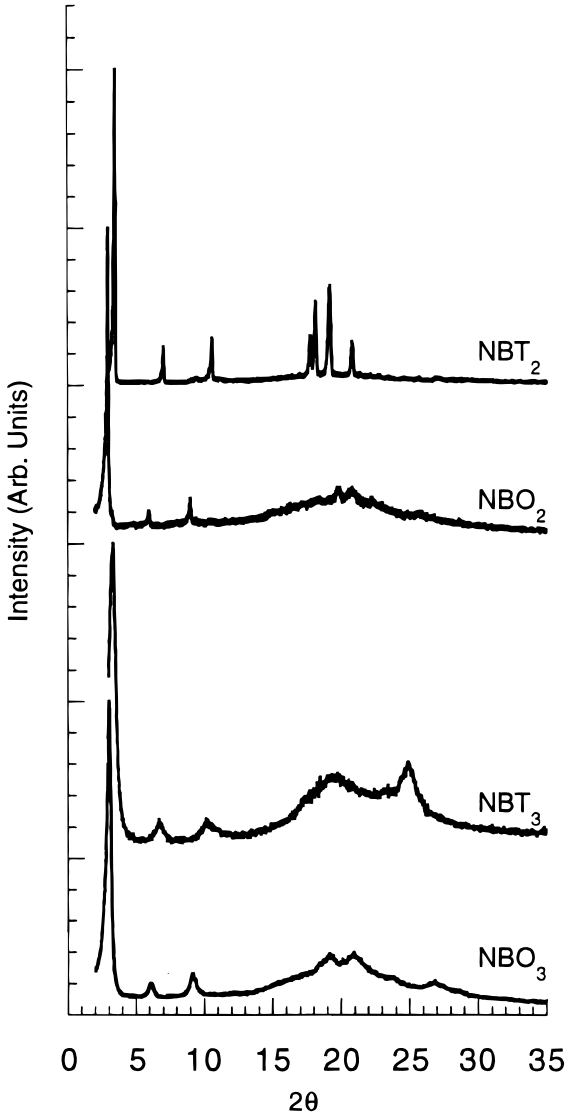


**Figure 12.** XRD patterns for $NBT_2$, $NBO_2$, $NBT_3$, and $NBO_3$.

Although NBT and NBO have differences in their solid-state packing, the higher oligomers of both systems

(49) DeWitt, L.; Blanchard, G. J.; LeGoff, E.; Benz, M. E.; Liao, J. H.; Kanatzidis, M. G. *J. Am. Chem. Soc.* **1993**, *115*, 12158.
(50) Meille, S. V.; Farina, A.; Bezziccheri, F.; Gallazzi, M. C. *Adv. Mater.* **1994**, *6*, 848.
(51) Douglas, B. E.; McDaniel, D. H.; Alexander, J. J. *Concepts and Models of Inorganic Chemistry*, 2nd ed.; John Wiley & Sons: New York, 1983.

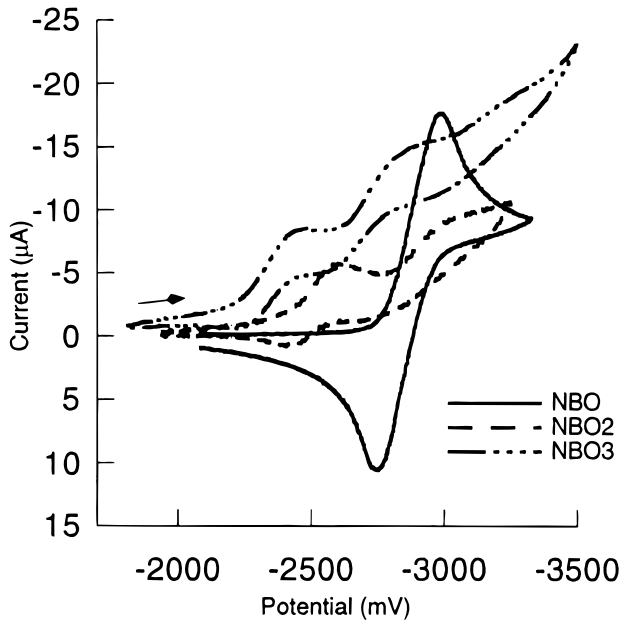


**Figure 13.** CV spectra for NBO, $NBO_2$, and $NBO_3$ solutions (vs $Fc/Fc^+$).

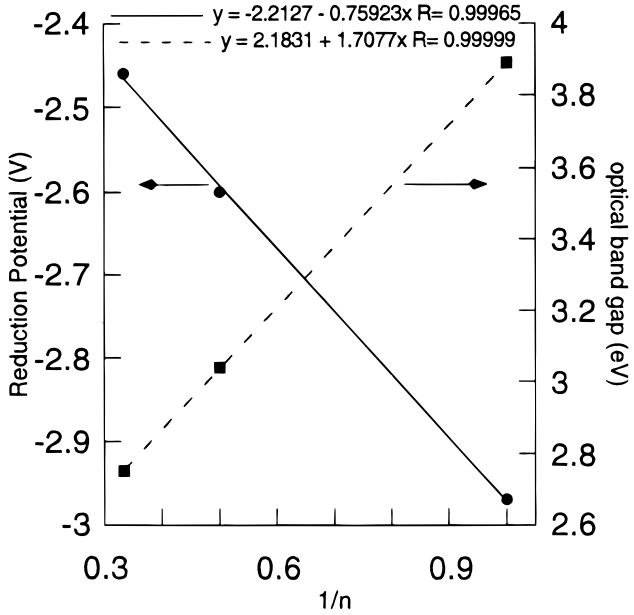


**Figure 14.** Plots of the first reduction potentials and optical band gap vs 1/*n* for NBO, $NBO_2$, and $NBO_3$ solutions.

**Table 4. Reduction Potential Values**[a]

| oligomer | $E_p^R$ | $E_{p/2}$ | $\Delta E_p$ |
|---|---|---|---|
| NBO | −2.97 | −2.85 | 0.24 |
| $NBO_2$ | | | |
| $E_1$ | −2.60 | −2.54 | 0.18 |
| $E_2$ | −3.03 | −2.88 | 0.31 |
| $NBO_3$ | | | |
| $E_1$ | −2.46 | −2.35 | 0.28 |
| $E_2$ | −2.91 | −2.75 | 0.33 |
| $E_3$ | −3.30 | −3.18 | 0.25 |

[a] The values are reported vs the $Fc/Fc^+$ couple.

appear to pack in a similar manner. Figure 12 overlays the XRD patterns of $NBO_2$, $NBO_3$, $NBT_2$, and $NBT_3$. All of the compounds exhibit first-, second-, and third-order peaks for the interchain, lamellar spacing. As the chain length increases, so does the lamellar spacing: 23.04, 25.43, and 26.58 Å for $n = 1, 2, 3$, respectively, in $NBT_n$.

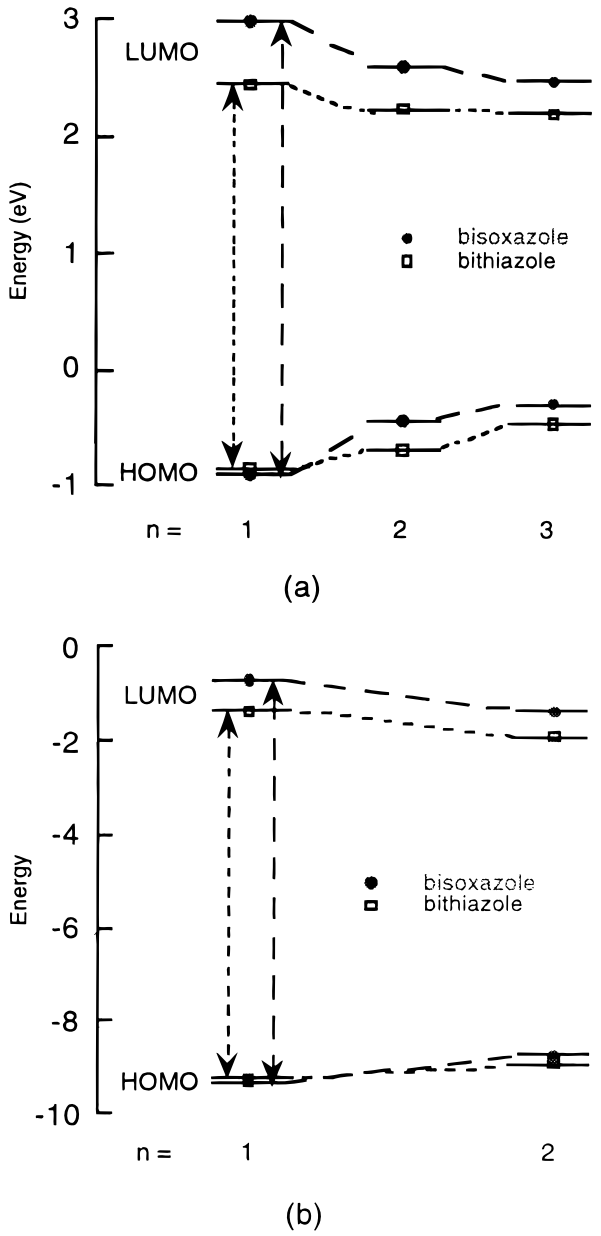


**Figure 15.** (a) The relative energy levels of the HOMOs and LUMOs for both the NBO and NBT oligomers as defined by CV and UV−vis. (b) Calculated energy levels of the HOMOs and LUMOs for MBO, $MBO_2$, MBT, and $MBT_2$ as calculated by MOPAC.

Assuming a fully extended alkyl chain in the all-trans conformation, these data suggest either a decrease in the dihedral angle between the chain and the ring (toward a more planar molecule), or a subtle change in the orientation of the molecules with respect to the cell edge. The observed lamellar spacing for both $NBO_2$ and $NBO_3$ is 29.22 Å, which is slightly longer than the end-to-end distance of NBO, 28.70 Å. The lamellar spacings for $NBO_2$ and $NBO_3$ may be the same because the side chains are fully extended and coplanar as seen in the structure of NBO.

**Electrochemical Behavior.** The cyclic voltammetry (CV) measurements of the NBO oligomers were obtained for comparison to the NBT oligomers. Figure 13 overlays the reduction waves of the three materials and Table 4 summarizes the reduction potentials. NBO has a quasi-reversible reduction, $E_pR = -2.97$ V ($E_{p/2} = -2.85$ V,

$\Delta E_p = 240$ mV), in both $CH_3CN$ and THF. In $CH_3CN$, the reduction is less reversible and is at the edge of the solvent window. $NBO_2$ shows two resolvable reduction waves in THF (the oligomers are not soluble in $CH_3CN$) at $E_pR = -2.60$ and $-3.03$ V and two return oxidation waves at $-2.42$ and $-2.72$ V ($\Delta E_1 = 180$ mV, $\Delta E_2 = 310$ mV). The trimer has three poorly resolved reduction peaks at $E_pR = -2.46$, $-2.91$, and $-3.30$ V, and three discernible reoxidation peaks at $-2.18$, $-2.58$, and $-3.05$ V ($\Delta E_p = 280$, 330, and 250 mV, respectively).

The reduction potential becomes more positive with increasing length of the oligomer. A graph of the first reduction potentials vs $1/n$ ($n$ = number of bisoxazole units) can be fit to a straight line. This behavior is not surprising because the HOMO−LUMO gap of these oligomers also scales with $1/n$, and the reduction potential is related to the energy of the LUMO. Figure 14 overlays the plot of both the first reduction potential and the optical band gap vs $1/n$.

These electrochemical results suggest that one electron can be added for each NBO unit in the oligomer. NBT oligomers also exhibit one, two, and three reduction peaks for $n = 1$, 2, and 3, respectively.[38] However, the first two reduction peaks of $NBT_3$ are merging into a single broad peak. The separation of reduction peaks is caused by a strong interaction between reducible centers. Compared to $NBO_3$, the merging of the reduction peaks in $NBT_3$ is indicative of less electronic communication between the reducible centers, possibly caused by larger twist angles between the bithiazole rings in solution as deduced from the absorption spectra. The increased planarity of $NBO_3$ lengthens the effective conjugation and maintains stronger interaction between reducible centers than in $NBT_3$. Only two reduction peaks are observed in $NBT_5$. Theory predicts that only two CV peaks should be present in longer polymers of interacting, redox-active centers.[52]

Figure 15(a) shows the relative energy levels of the HOMOs and LUMOs as calculated from the first reduction peak and the optical band gap. The optical band gap was found from the solution UV−vis spectra by extrapolation of the low energy portion of the curve to $y = 0$. The figure shows that NBO has a higher energy LUMO as well as a lower energy HOMO, resulting in the higher reduction and oxidation potentials vs NBT. NBO irreversibly oxidizes at 1.6 V, whereas NBT irreversibly oxidizes at 1.3 V. In $NBO_2$, the HOMO has a higher energy than the HOMO of $NBT_2$ because of the greater band dispersion caused by higher AO coefficients at the 5,5′-positions of the HOMO of NBO in relation to NBT (see above); however, the relative positions of the LUMOs remain the same. This switching of the relative positions of the HOMOs was predicted in the MOPAC calculations as shown in Figure 15(b).

## Conclusions

The structures and optoelectronic properties of a series of oxygen- or sulfur-containing heterocycles were compared. NBO molecules associate into "$\pi$-dimers" that pack in infinite, H-bonded, two-layered ribbons, whereas NBT forms infinite "staircases" of slipped $\pi$-stacks with short interstack S···S contacts. Such features are important for determining charge transport properties of polymers prepared from the NBO or NBT ring systems. The NBO-based oligomers appear to be more planar in solution than their NBT counterparts. Spectral and cyclic voltammetric data were interpreted with the aid of MO theory. The oxygen-for-sulfur substitution lowers the HOMO and raises the LUMO in NBO relative to NBT, but the HOMO−HOMO interaction in NBO−NBO is larger than that in NBT−NBT, leading to an inversion in the HOMO energies in the higher oligomers. Knowledge of the electronic structure and molecular packing aids in the design of polymers for use in thin film transistors and other devices.

**Acknowledgment.** The authors thank the National Science Foundation (DMR-9510274) for support for this research and J. I. Nanos for information involving $(NBT)_n$.

**Supporting Information Available:** Complete X-ray crystallographic tables for NBO and the synthesis of $NBT_2$. This material is available free of charge via the Internet at http://pubs.acs.org.

CM990278U

(52) Aoki, K.; Chen, J. *J. Electroanal. Chem.* **1995**, *380*, 35.